A FULLY AUTOMATED CAD-BASED FRAMEWORK FOR SHAPE OPTIMIZATION

Keita Hatanaka*, Joel Brezillon**, Arno Ronzheimer**
*Mitsubishi Aircraft Corporation, **German Aerospace Center
keita_hatanaka@mitsubishiaircraft.com
Joel.Brezillon@dlr.de, *Arno.Ronzheimer@dlr.de*

Keywords: *Optimization, NURBS, CAD, MDO*

Abstract

In the area of aircraft design, many studies about Multi Disciplinary Optimization (MDO) and Multi Objective Optimization (MOO) have been published in the last decade. However, there are some concerns that prevent the use of many developed optimization tools in a real aircraft design process. These issues are simply a lack of functionalities of treating surface/surface intersections and geometrical constraints, and difficulties of applying design knowledge to the real aircraft design that are the fundamental features for MDO and MOO. In this study, a new shape parameterization framework is proposed to overcome these issues by establishing a geometry parameterization method based on a NURBS formulation that is used in nearly any state of the art CAD software, and utilizing the Free Form Deformation technique to deform the aircraft shapes arbitrary with a moderate number of design variables. With the developed shape parameterization based on NURBS in combination with a newly developed surface grid deformation approach optimizations have been carried out for the DLR-F6 wing-body-nacelle-pylon configuration. A significant drag minimization has been achieved in cases with and without geometrical constraints. It is demonstrated that this approach will be an essential design tool in practical aircraft design.

1 Introduction

In the field of shape optimization, the geometry representation plays an important roll and it strongly affects the ease of applying of design knowledge to the real aircraft design process after shape optimization. Numerous methods (Ref. [1]–[5]) have been devised to numerically represent geometries to be used in aerodynamic design, optimization, and also for parametric studies. With regard to the wing shape definition, for example, Hicks-Henne shape function (Ref. [2]), PARSEC (Ref. [3]) and spline-based representations are widely used for sectional airfoil shape representation and for shape modification. Then, a span-wise connection of airfoils to form a wing loft is typically calculated by a simple interpolation of polynomial or spline-based methods. In such mathematical representations, CST (Ref. [4]) is a systematic method proposed as a universal parametric geometry representation method for nearly all aircraft components. CST is developed to allow the specification of meaningful design parameters such as leading-edge radius, boat-tail angle and airfoil closure angle directly. However, these parameterization methods are not mature enough from a shape design stand point. To be used as a practical design tool, the capability of treating intersections and complex geometrical constraints are mandatory, and an ease of transferring design knowledge into design process is also a key feature.

In this study, a new geometry representation framework based on NURBS, (Ref. [6]) which has become a common CAD format in any industrial field is proposed. In this framework, NURBS is used to exchange the geometry data between 3D CAD software and the optimization tool easily.

2 Shape representation approach

2.1 NURBS Surface

A Non-Uniform Rational B-Spline (NURBS) is a de-facto industry standard for a free-form shape representation and has been applied to the wide variety of CAD software. By using the NURBS representation method, C^{m-2} continuity is guaranteed in the whole region of the surface. A NURBS surface is represented by the coordinates of the control points and weights. The basis function reads as follows;

$$\bar{P}(u,v) \equiv (x(u,v), y(u,v), z(u,v)) = \frac{\displaystyle\sum_{i=0}^{nu-1}\sum_{j=0}^{nv-1} N_{i,mu}(u) N_{j,mv}(v) \omega_{ij} \bar{Q}_{ij}}{\displaystyle\sum_{i=0}^{nu-1}\sum_{j=0}^{nv-1} N_{i,mu}(u) N_{j,mv}(v) \omega_{ij}}$$

$$u_0 \le u \le u_{nu+mu-1}$$

$$v_0 \le v \le v_{nv+mv-1}$$

mu, mv : Order of the NURBS function for UV directions

nu, nv : Number of control points for UV directions

$N_{i,mu}, N_{j,mv}$: Basis function for UV directions

$\bar{Q}_{ij}$: control points for NURBS surface

u, v : Parameter for UV directions

u_i, v_j : Knot vector for UV directions

ω_{ij} : Weight vector of each control point

The Basis function is as follows.

$$N_{i,1}(u) = \begin{cases} 1 & (u_i \le u < u_{i+1}) \\ 0 & (u < u_i, u_{i+1} \le u) \end{cases}$$

$$N_{i,m}(u) = \frac{u - u_i}{u_{i+mu-1} - u_i} N_{i,mu-1}(u) + \frac{u_{i+mu} - u}{u_{i+mu} - u_{i+1}} N_{i+1,mu-1}(u)$$

$$N_{j,1}(v) = \begin{cases} 1 & (v_j \le v < v_{j+1}) \\ 0 & (v < v_j, v_{j+1} \le v) \end{cases}$$

$$N_{j,mv}(v) = \frac{v - v_j}{v_{j+mv-1} - v_j} N_{j,mv-1}(v) + \frac{v_{j+mv} - v}{v_{j+mv} - v_{j+1}} N_{j+1,mv-1}(v)$$

The shape can be modified by either changing the position of the control points or by changing the weights.

2.2 Free Form Deformation

As described in the previous section, NURBS surface is expressed as a mixture of the coordinates of the control points and weights, and the number of control points depends on the complexity and the order of the surface. In the practical field, the number of control points usually exceeds 100 and sometimes it may reach one thousand. From the optimization point of view, less design variables are better to reduce the computational resources. In this study, to deform a NURBS surface, a Free Form Deformation (FFD) technique, which was originally developed in the computer graphics field and has been enhanced to be used with an optimization loop at DLR (Ref. [7]), was applied. This method is based on a B-Spline function rather than the NURBS function to achieve both simplification of the deformation process and reduction of the computational complexity. Basic principle of the FFD technique is a mapping and re-mapping of point coordinates into and from B-spline volumes. The deformation is achieved indirectly by changing the coordinates of the control points of the B-spline volume. The FFD technique allows a user to get more smooth and coherent deformation by less design variables. Fig. 1 shows an example of the FFD result which is applied to a NURBS surface. In this case, it is clearly observed that by changing the control points of the B-spline volume rather than changing the control points of NURBS surface directly, NURBS surface can be deformed.

A B-spline volume can be expressed as follows;

$$\bar{P}(u,v,w) = \sum_{i=0}^{nu-1}\sum_{j=0}^{nv-1}\sum_{k=0}^{nw-1} N_{i,mu}(u) N_{j,mv}(v) N_{k,mw}(w) \bar{Q}_{ijk}$$

$$\begin{cases} u_0 \le u \le u_{nu+mu-1} \\ v_0 \le v \le v_{nv+mv-1} \\ w_0 \le w \le w_{nw+mw-1} \end{cases}$$

mu, mv, mw : Order of the B-spline function for UVW directions

nu, nv, nw : Number of control points for UVW directions

$N_{i,mu}$, $N_{j,mv}$, $N_{k,mw}$: Basis function for UVW directions

Q_{ijk} : control points for B-spline volume

u, v, w : Parameter for UVW directions

u_i, v_j, w_k : Knot vector for UVW directions

The Basis functions are derived in the same way as 1.1.

2.3 Surface/Surface intersection

Surface/Surface intersection is a fundamental feature in the CAD and Computer Aided Geometric Design (CAGD) fields, and this is a complex subject that has been an active research field for more than three decades. In this study, a subdivision algorithm (Ref. [8]) was implemented to achieve an automatic and robust intersection calculation between two surfaces during shape optimization. The main advantage of this algorithm is that it is applicable to any surface representations such as NURBS surface, B-Spline surface, Bezier surface and so on. Moreover, it is independent of the shape and complexity of the intersection curves. Fig. 2 shows an intersection calculation process of this algorithm.

This algorithm involves four steps:

- Subdivision – Both surfaces are subdivided into a number of squares, and then each piece will be subdivided again if the piece is close to another surface. This subdivision process is done on the parametric space as shown in Fig. 2. In this process, those squares, which have possibilities to have an intersection, will be subdivided.

- Intersection – Both NURBS surfaces are assumed as the collection of the triangle meshes where each square in the previous process is composed of two triangles. Then intersection segments will be evaluated as shown in Fig. 2.

- Projection – Both edge points of the intersection segments from the previous process are not lying on the exact surface because the NURBS surfaces were assumed as the triangle meshes. In this process, both edge points of the intersection segments will be projected on both surfaces.

- Construction – By using all intersection points, an intersection curve for both 3D space and the UV parametric space can be constructed.

2.4 Geometrical constraints

Considering geometrical constraints in a shape optimization is a key issue for the practical application to maintain the feasibility of the optimized geometry, and it has become also an active research field in shape optimization. One solution to apply a geometrical constraint is to limit the design space itself. However, to find a proper design space so that the geometry does not violate a constraint is not an easy task for designers. In this study, a more practical way for a consideration of geometrical constraints was implemented by being coupled with the sequential quadratic programming (SQP) (Ref. [9]). In this method, the designer has to create a surface that should not be violated during the optimization. Fig. 3 shows a spar surface in the wing geometry as an example of the geometrical constraints. The area of these spar surfaces are calculated at the beginning of the shape optimization, and the optimizer tries to keep these area constant during the optimization process. When the wing becomes thinner, these surfaces will be exposed outside, which is shown in Fig. 3. This means the areas of the spar surfaces are smaller than the initial value. The constraints checker will calculate the difference between the initial value and the current value, and the optimizer will produce a next design vector to reduce this difference.

2.5 Process chain with novel mesh deformation

Fig. 4 shows a complete flow chart of the proposed framework for a shape optimization. The proposed framework involves three main steps, [initialization], [update] and [evaluation] steps. In early approaches after deformation of the surface the mesh is newly generated, what is time consuming and disables the application of an adjoint method. Here a sophisticated mapping procedure to a Delauny triangulation of the UV space has been established which allows an immediate recalculation of the surface mesh after deformation and calculation of intersections.

1) [Initialization] process.
   The main purpose of this process is to establish a relation between the parametric space (UV for a NURBS surface and UVW for a B-spline volume) and XYZ space. This process works as follows:

   i. All control points of the NURBS surfaces are mapped into the B-spline volume. UVW parameters are also assigned to every control points and these UVW parameters are stored for the [update] process.

   ii. All mesh points are projected onto the NURBS surface and UV parameters are assigned and stored. (Fig. 5)

   iii. The length ratio of the mesh points on the intersection curve described below is calculated and stored.

   During the optimization, the length ratio should always be kept, and in the [update] process, the new mesh points on the updated intersection curve are re-calculated based on the length ratio.
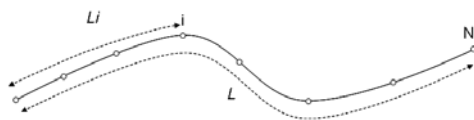
Length ratio $r_i = \dfrac{L_i}{L}$

L_i : length from start point to ith point

L : whole curve length

2) [Update] process.
   The design variables coming from an optimizer change the coordinates of control points of the B-spline volume that leads the surface mesh modification. Then the volume mesh is deformed according to the change of the surface mesh. The process goes as follows:

   i. The coordinates of control points of the B-spline volume are changed by the design variables.

   ii. The control points of the NURBS surface are recalculated by using the UVW parameter derived from the [initialization] process and the updated control points of the B-spline volume.

   iii. New intersection curves are calculated by using the updated NURBS surface.

   iv. The new mesh points on the intersection curve are calculated based on the length ratio.

   v. Surface mesh is deformed in the UV space and new UV parameters are calculated (Fig. 6). In this process, to achieve a robust and fast mesh deformation, a Delaunay graph mapping method for 2D problems (Ref. [10]) was adopted. This mesh deformation is done on the UV coordinate, not on the XYZ coordinate. As a first step, UV space is filled with Delaunay triangles (Fig. 7) and then the relation between the Delaunay triangles and the mesh points is established. At each design step, an intersection is modified and then, by using that relation, new mesh UV parameters are calculated.

   vi. New surface mesh points are calculated (Fig. 8) by using updated NURBS surfaces derived from process ii, and the updated UV parameters derived from process v.

   vii. The displacement of the surface mesh is propagated into the volume mesh and the new volume mesh points are calculated by using a volume mesh deformation tool (Ref. [11]). (Fig. 9)

3) [Evaluation] process

In this process, all the parameters, an objective function, constraints and the gradient, that are required for the optimizer are calculated. The details of each evaluation method are described in the next section.

The major benefit of this flow chart is having the CAD representation within the optimization loop, and the final geometry is directly usable for other process without lengthy CAD conversion.

3 Design tools

The shape representation tool of the previous section is coupled with an aerodynamic design optimization system composed of an unstructured flow solver, a discrete adjoint code, and gradient-based optimizers.

3.1 Flow and sensitivity analysis

The TAU-Euler code, a three-dimensional unstructured Euler solver (Ref. [12], [13]), was used for the compressible flow analysis, and for the Adjoint flow problem, a discrete Adjoint of TAU was used. (Ref. [14], [15]).

3.2 Optimization algorithm

In this study, two gradient-based optimization methods utilizing the gradient of the objective functions provided by the Adjoint solver were applied. For an optimization without constraints, the Conjugate Gradient (CG) method with line-searches was used to solve a drag minimization problem, and for a constrained optimization, the Sequential Quadratic Programming (SQP) method with the objective function approximated by a quadratic Taylor series expansion was used to create a direction-finding problem. Detailed algorithms and methodologies of the SQP method are described in Ref. [9]. To automate the whole optimization process, the proposed framework was coupled with "Pyranha" (Ref. [16]), a python based optimization framework that has been developed in DLR.

4 Design Examples

An installation of engine components has significant effects on aircraft performances especially at a high speed condition. Mitsubishi Aircraft Corporation and Tohoku University have studied intensively on the engine-airframe integration with MDO and aerodynamic design optimization approaches in past research activities (Ref. [17],[18]).

As a design example of an aircraft configuration with under wing mounted engines, the present method was applied to DLR-F6 wing-body-nacelle-pylon configuration (Ref. [19]), a generic twin-jet transport aircraft configuration, as shown in Fig. 10. The computational mesh for this configuration contains about 0.6 million tetrahedras. The surface mesh was generated by the direct advancing front method coupled with the geometrical feature extraction on the STL (Stereo lithography) data format. (Ref. [20]) The tetrahedral volume mesh was generated by a Delaunay-type generation method. (Ref. [21])

4.1 DLR-F6 WBNP configuration without geometrical constraints

Design conditions are free stream Mach number of 0.85 and a lift coefficient CL of 0.625. The objective of this design example is to minimize a drag coefficient at the fixed Mach and lift coefficient. In total, 96 design variables were used for the free form deformation of the wing geometry. The FFD box and the surface mesh are shown in Fig. 11.

To have a greater flexibility to deform the geometry around the leading edge region, the FFD box node was concentrated around the leading edge region. Geometrical constraints were not explicitly imposed in this case. The magnitude of the displacement was set +/- 3% of the each chord length by setting the domain of each design variable. In total, 16 times Euler analysis and 8 times Adjoint analysis were conducted using the HPC cluster in DLR.

It took 15 minutes per Euler analysis and 30 minutes per Adjoint analysis to converge the residual up to 1.0e-6 for the Euler analysis and 1.0e-8 for the Adjoint analysis. In total, it took 8 hours for the whole design.

Fig. 12 shows the history of the design optimization. With the optimization, a drag reduction of more than 110 drag cts (Δ CD=0.0110) was achieved. Fig. 13 shows the comparison of the surface pressure distribution and Fig. 14 shows the comparison of the airfoil section and sectional pressure distribution between the baseline and the optimized geometry with minimum drag. From Fig 13, it can be clearly observed that the designed geometry has lower pressure around the leading edge region at both inboard and outboard sections. As seen in Fig. 14, to achieve the pressure change described above, the curvature around the leading edge was increased and that of trailing edge was decreased.

4.2 DLR-F6 WBNP configuration with geometrical constraints

As a next design example, the same configuration, however with geometrical constraints, was chosen to demonstrate the optimization capability under the constrained condition. Design conditions are the same values as the previous design optimization. The objective function of this design example is also to minimize the drag coefficient at a fixed Mach number and a fixed lift coefficient. In total, 96 design variables were used for the free form deformation of the wing geometry. As seen in Fig. 15, several surfaces at the spar location such as a front spar, a rear spar and an auxiliary spar were created for the geometrical constraints. As described in Section 1.4, the initial areas of these spar surfaces were calculated at the beginning and these value were used as the target area during the optimization. This means that even if the wing shape is changed by the optimizer, the area of these spar surfaces will be kept. At each design step, the area differences of the predefined surfaces for the geometrical constraints, between the designed geometry and the original geometry are calculated. And then, based on that information, the optimizer can provide a new design vector that reduces area differences for the next geometry.

Fig. 16 shows the optimization history. With the optimization, 50 drag cts (Δ CD=0.0050) reduction was achieved under the constrained conditions. Fig. 17 shows the comparison of the surface pressure distribution and Fig. 18 shows the comparison of the airfoil section and sectional pressure distribution between the baseline and the optimized geometry that has a minimum drag. In Fig 18, vertical lines show the spar location.

Even though the resultant shape does not differ from the baseline due to the constraints, the trend of the change of the pressure distributions are close to that of the previous design example. The suction peak around the leading edge was increased and the acceleration at the trailing edge region was suppressed. Both changes have contributed to the drag reduction.

5   Conclusion

In this study, a new CAD-based shape parameterization framework that incorporates NURBS formulation for smooth surface/curve representation coupled with the Adjoint method is proposed. The general approach of the presented work is to establish a practical optimization framework that can take into account a change of the intersection curve between two geometries.

To demonstrate the applicability of the framework for practical design task, a geometry such as the wing-body-nacelle-pylon DLR-F6 configuration was adopted.

The method for applying the geometrical constraints to the shape optimization is also described and that capability is presented by means of the shape optimization with and without geometrical constraints.

For the shape optimization of DLR-F6 WBNP configuration without any geometrical constraints, it is shown that the proposed framework is applicable for the shape deformation of the complex geometry, and more than 100 drag counts reduction can be achieved by that optimization.

For the optimization with the geometrical constraints, which limits the spar thickness of the wing structure, it is shown that the optimizer is able to find an optimum within the limited design space and 50 drag counts reduction can be achieved by that optimization.

Since the IGES format is chosen as geometry container in this optimization framework, the optimized geometry can be transferred back from the optimization framework to the practical aircraft design process with CAD/CAE methods rapidly. As a result, designers don't have to take their time for applying design knowledge to the real aircraft design manually and this tool enables them to focus on the phenomena and the design process. As a future work, it is intended to implement "trimmed surface" in this framework.

References

[1] Samareh, J. A., "Survey of Shape Parameterization Techniques for High-Fidelity Multidisciplinary Shape Optimization," AIAA Journal,Vol. 39, No. 5, pp. 877–884, 2002.

[2] Hicks, R. M., and Henne, P. A., "Wing Design by Numerical Optimization," Journal of Aircraft, Vol. 15, No. 7, pp. 407–412, 1978.

[3] Sobieczky, H., "Parametric Airfoils and Wings," Notes on Numerical Fluid Mechanics, pp. 71-88, Vieweg, 1998.

[4] Kulfan, M.B., "Universal Parametric Geometry Representation Method," Journal of Aircraft, Vol.45, No.1, pp. 142-158, 2008.

[5] Jeong,S,. Obayashi, S., "Efficient Global Optimization (EGO) for Multi-Objective Problem and Data Mining", Evolutionary Computation, 2005. The 2005 IEEE Congress on In Evolutionary Computation, 2005. The 2005 IEEE Congress on, Vol. 3 (2005), pp. 2138-2145 Vol. 3.

[6] Les, P., and Wayne, T., The NURBS Book, 2nd ed., Springer-Verlag, Belrin, 1995, Chap. 14.

[7] Ronzheimer, A., "Post-Parametrisation of CAD-Geometries Using Freeform Deformation and Grid generation Techniques," Notes on Numerical Fluid Mechanics and multidisciplinary Design, Vol. 87, 2002, pp. 382-389.

[8] Teixeira, F. G., Creus, G. J., "A robust algorithm to determine surface/surface intersection in both parametric spaces," Mecánica Computacional, Vol. XXVII, 2008, pp. 3093–3115

[9] Jorge, N., and Stephen, J. W., Numerical Optimization, 2nd ed., Springer series in operations research, Springer-Verlag, New York, NY, 1999, Chap. 18.

[10] Xuequang, L., Ning, Q., and Hao, X., "Fast dynamic grid deformation based on Delaunay graph mapping," Journal of computational physics, Vol. 211, Issue. 2, 2006, pp. 405-423. doi: 10.1016

[11] Murayama, M., Nakahashi, K., and Matsushima, K., "A Robust Method for Unstructured Volume /Surface Mesh Movement," Transactions of the Japan Society for Aeronautical and Space Sciences, Vol. 46,No. 152, Aug. 2003, pp. 104–112.

[12] Gerhold, T., Galle, M., Friedrichs, O., and Evans, J., "Calculation of Complex Three-Dimensional Comfigurations employing the DLR TAU-Code," AIAA-97-0167, 1997.

[13] Schwamborn, D., Gerhold, T., and Heinrich, R., "The DLR TAU-Code: Recent Applications in Research and Industry," ECCOMAS CFD 2006, Egmond aan Zee, The Netherlands, September 5-8 2006.

[14] Dwight, R., Brezillon, J., and Vollmer, D., "Efficient Algorithms for Solution of the Adjoint Compressible Navier-Stokes Equations with Applications." Proceedings of the ONERA-DLR Aerospace Symposium (ODAS), Toulouse, 2006.

[15] Brezillon, J. and Dwight, R. P., "Discrete Adjoint of the Navier-Stokes Equations for Aerodynamic Shape Optimization," Evolutionary and Deterministic Methods for Design, edited by E. 2005, FLM, TU Munich, Germany, 2005.

[16] Brezillon, J., Ronzheimer, A., Haar, D., Abu-Zurayk, M., Lummer, M., Krüger, W. and Natterer, F. J., "Development and application of multi-disciplinary optimization capabilities based on high-fidelity methods," 8th AIAA Multidisciplinary Design Optimization Specialist Conference, 23-26 Apr. 2012, Honolulu, Hawaii.

[17] Takenaka, K,. Obayashi, S., Nakahashi, K., Matsushima, K., "The application of MDO Technologies to the Design of a High Performance Small Jet Aircraft - Lessons learned and some practical concerns -," AIAA paper 2005-4057, 2005.

[18] Saitoh, T., Kim, H., Takenaka, K.and Nakahashi, K., "Multi-Point Design of Wing-Body-Nacelle-Pylon Configuration," AIAA-2006-3461, 24th AIAA Applied Aerodynamics Conference in San Francisco, June 2006.

[19] Brodersen, O. und Stürmer, A., "Drag Prediction of Engine-Airframe Interference Effects using Unstructured Navier-Stokes Calculations," 19th AIAA Applied Aerodynamics Conference, 11-14 June 2001, Anaheim, CA, USA, AIAA 2001-2414.

[20] Ito, Y. and Nakahashi, K., "Direct Surface Triangulation Using Stereolithography Data," AIAA Journal., Vol. 40, No.3, 2002, pp.490-496.

[21] Sharov, D., Nakahashi, K., "A Boundary Recovery Algorithm for Delaunay Tetrahedral Meshing," 5th Int. Conf. On Numerical Grid Generation in Computational Field Simulations, 1996, pp. 229-238.
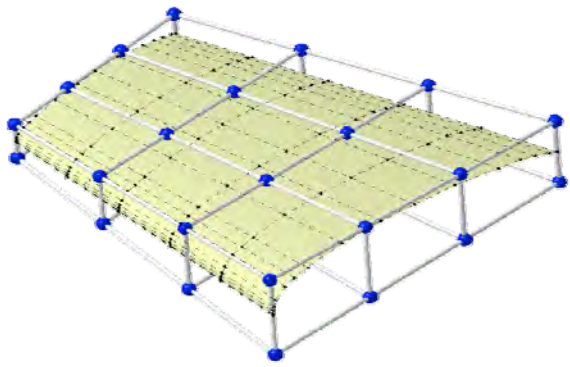
(a) before deformation
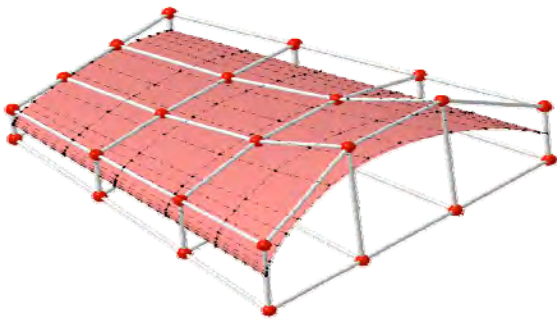
(b) after deformation
Fig.1 Deformed NURBS surface using Free
Form Deformation
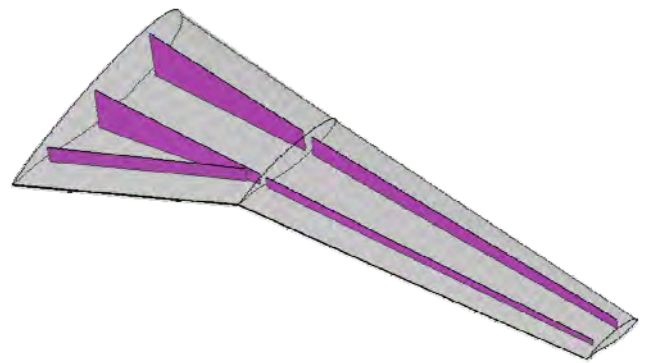
(a) spar surface in the wing geometry
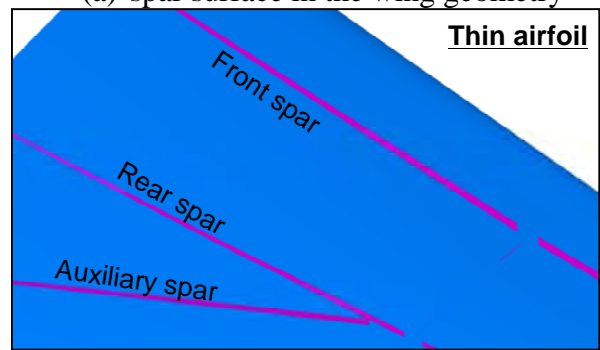
(b) exposed spar surface due to thinning the
wing geometry
Fig. 3 Geometrical constraints
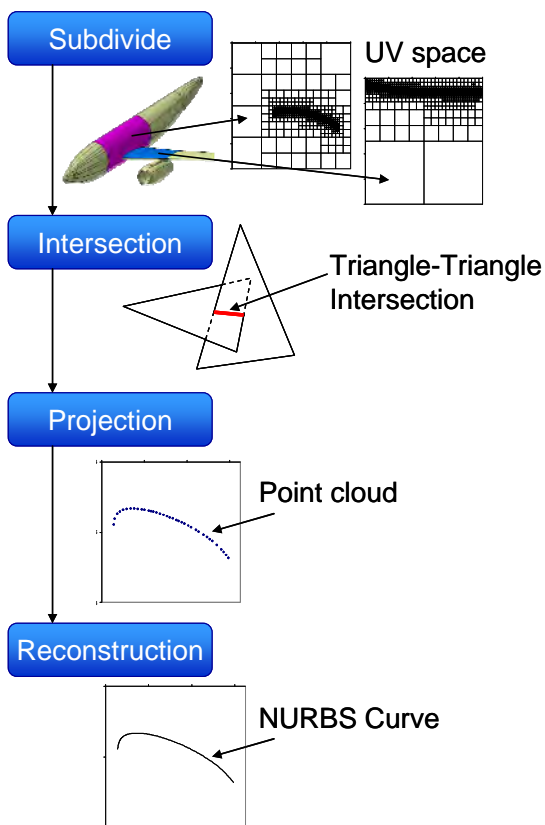
Fig. 2 Intersection calculation process
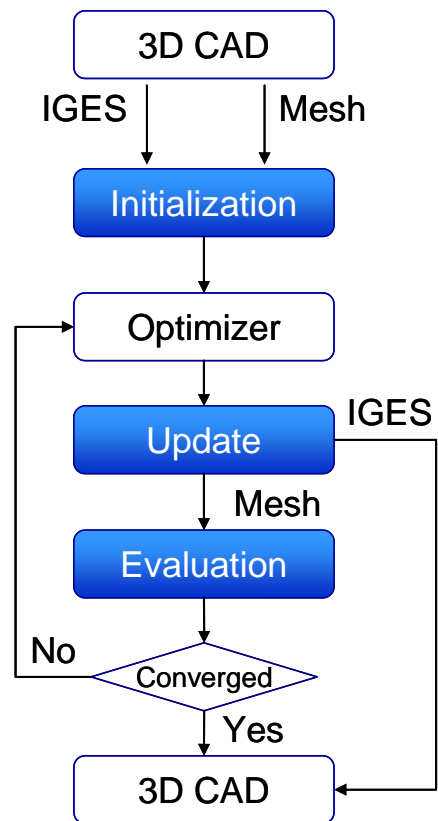
Fig.4 Optimization Process
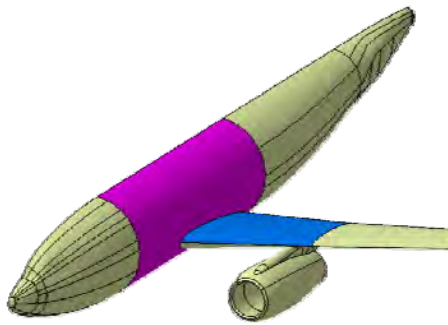
(a) NURBS surface where mesh points are
projected onto
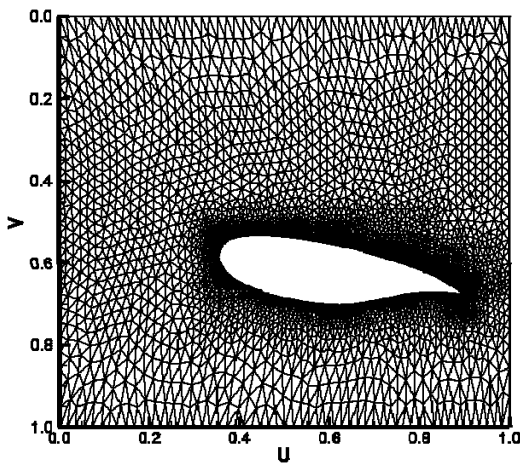
(b) mesh points projected on a fuselage surface
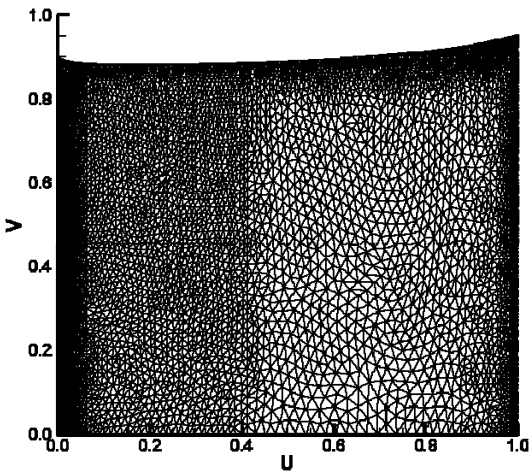
(c) mesh points projected on a wing surface
Fig. 5 Mesh points projected on NURBS surface
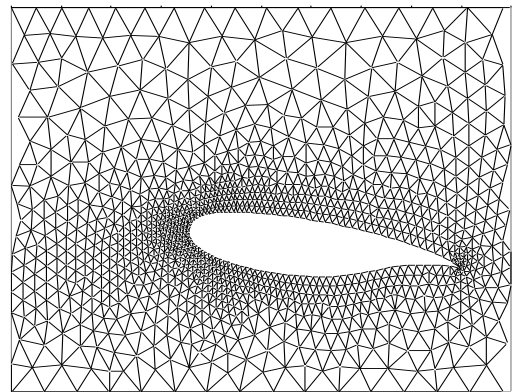
(a) baseline
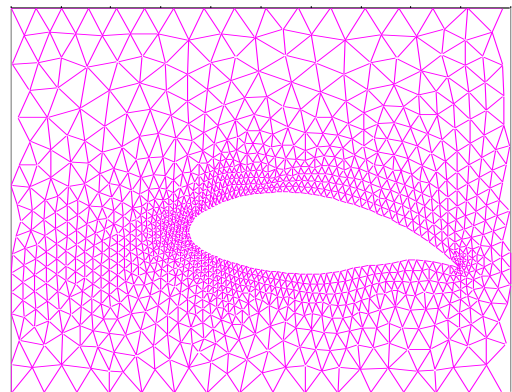
(b) deformed
Fig. 6 Deformed mesh in UV coordinate system
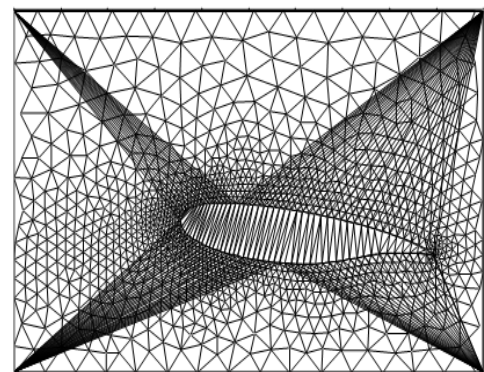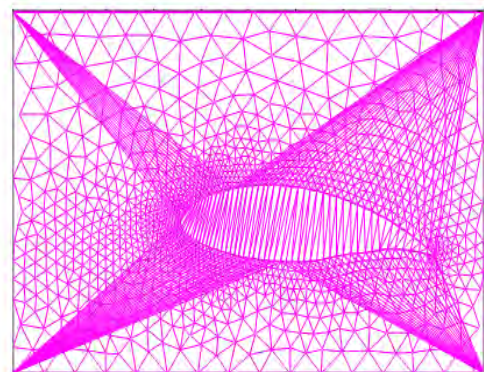
(a) baseline

(b) deformed
Fig. 7 Surface mesh with Delaunay triangles
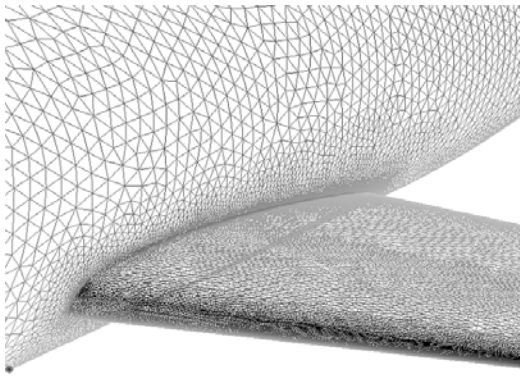
(a) baseline
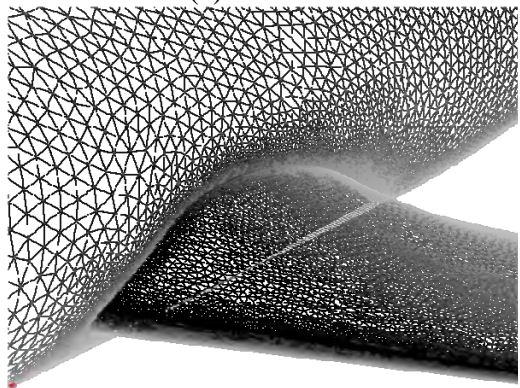
(b) deformed

Fig. 8 Deformed surface mesh in XYZ coordinate system
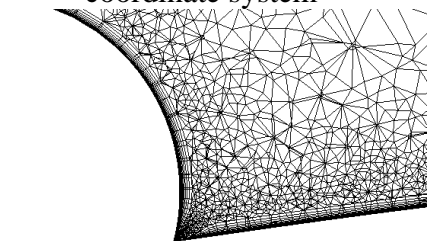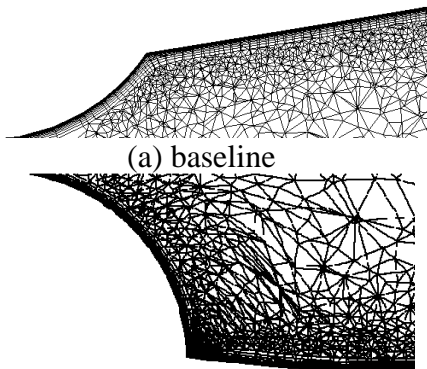
(a) baseline

(b) deformed

Fig. 9 Deformed volume mesh
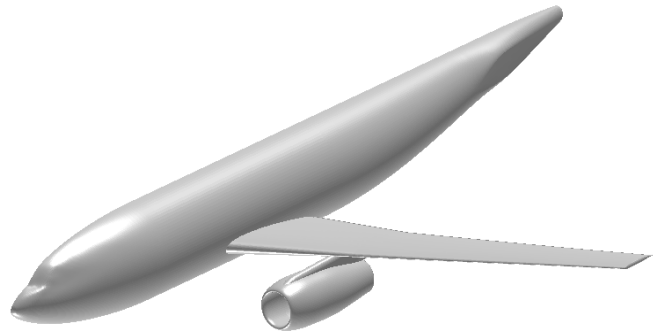
Fig. 10 DLR-F6 wing-body-nacelle-pylon configuration
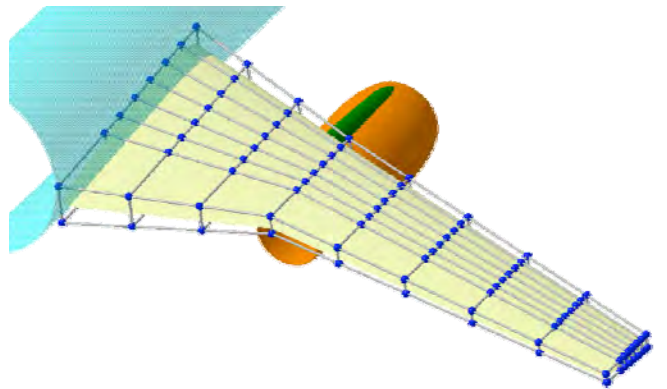
(a) FFD box
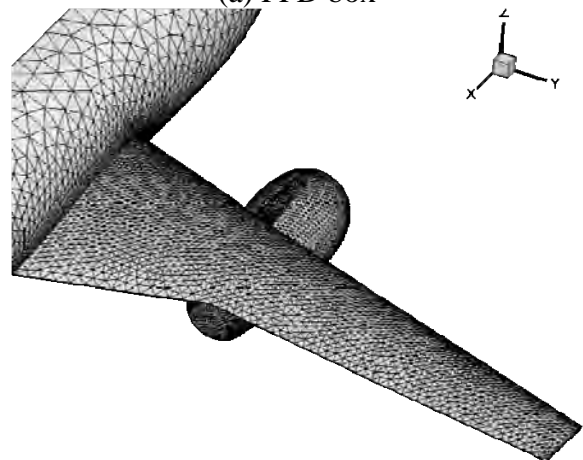
(b) surface mesh

Fig. 11 FFD box and the surface mesh on DLR-F6 configuration
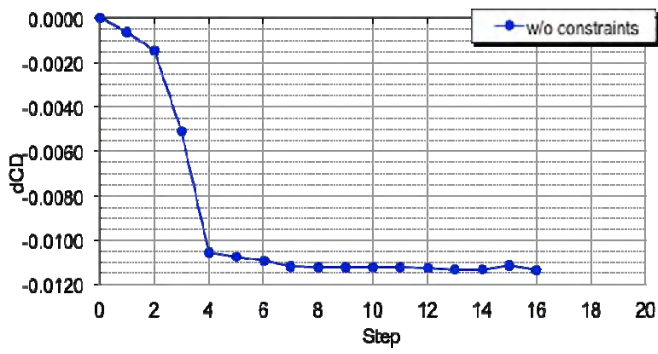
Fig. 12 History of the shape optimization without constraints
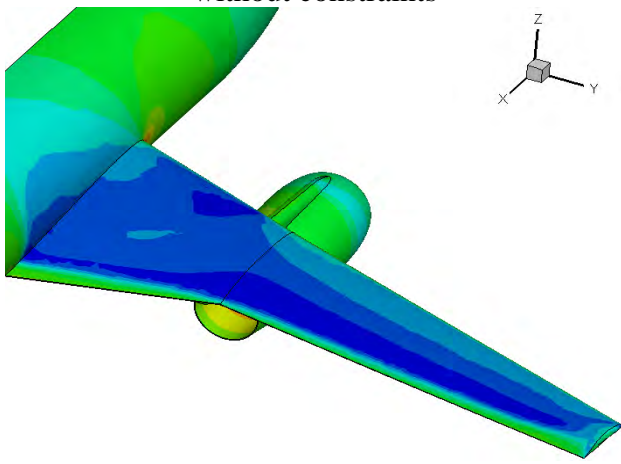
(a) baseline
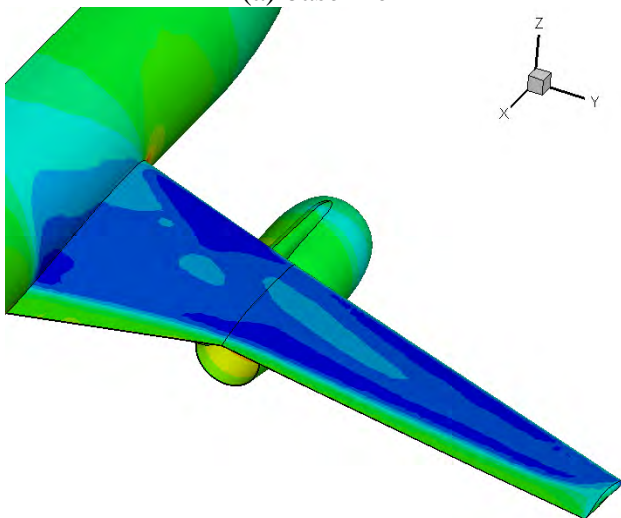
(b) optimized

Fig. 13 Comparison of the surface pressure distribution (w/o constraints)
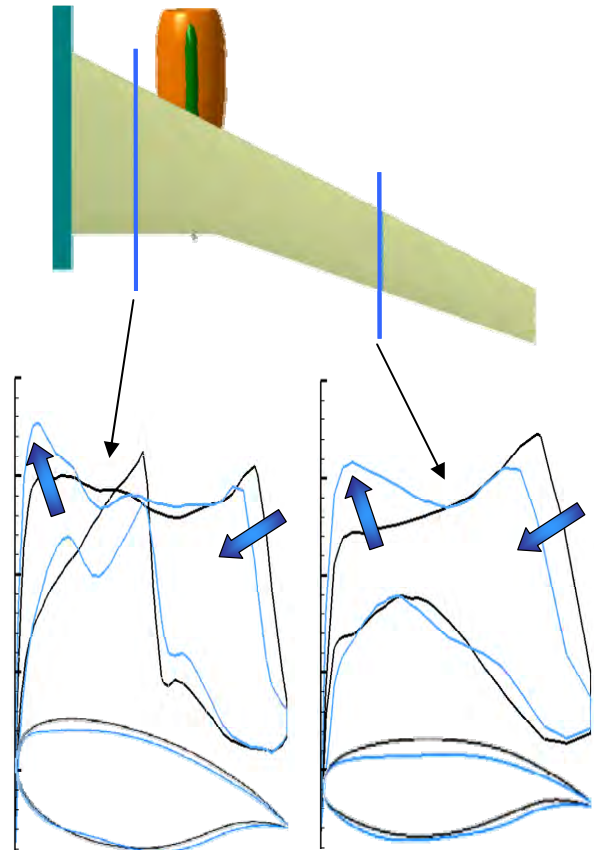
Fig. 14 Comparison of sectional airfoil and pressure distribution (w/o constraints)
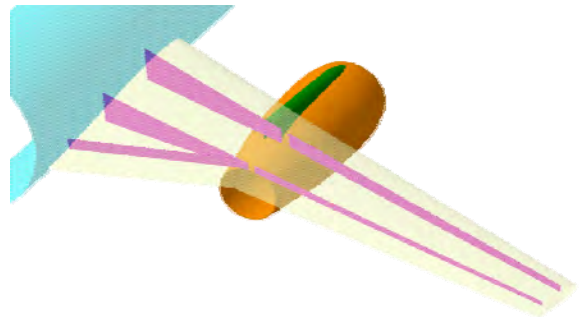
Fig. 15 Front, Rear and Auxiliary spar surfaces for the constraints
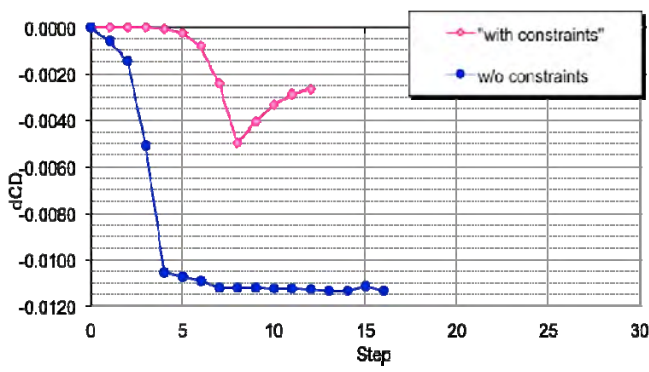
Fig. 16 History of the shape optimization
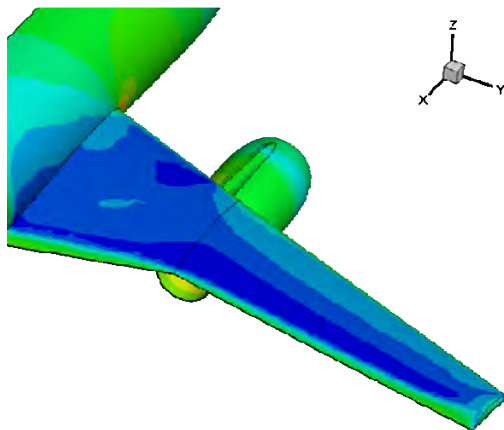
(a) baseline
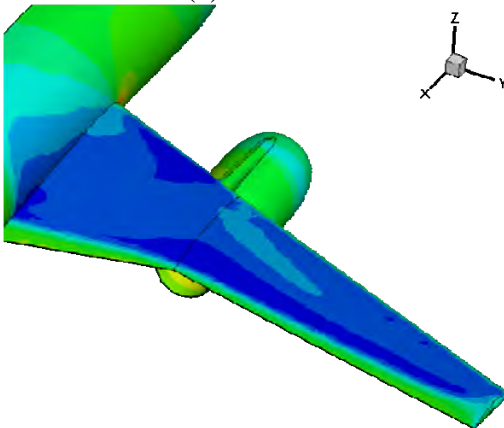
(b) optimized

Fig. 17 Comparison of the surface pressure distribution (with constraints)
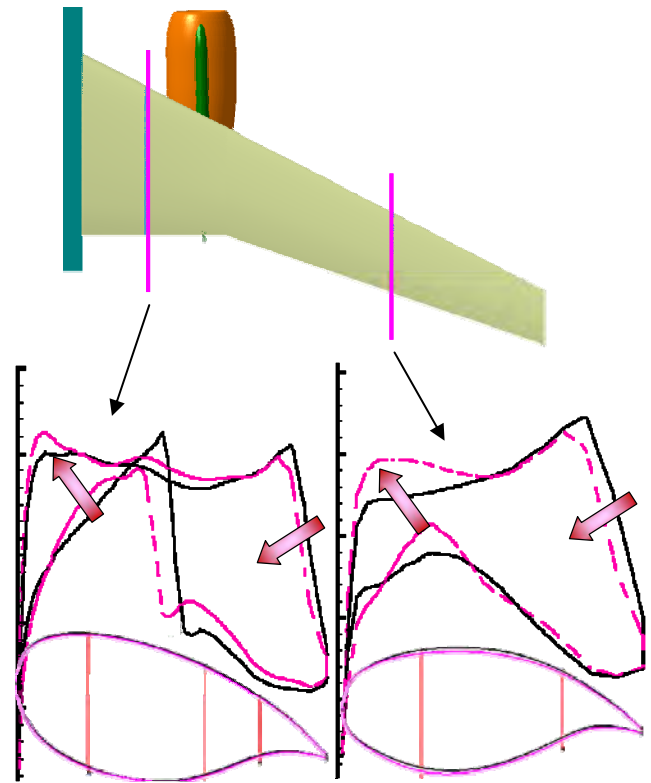
Fig. 18 Comparison of sectional airfoil and pressure distribution (with constraints)

Copyright Statement